Environmentally Assisted Cracking and Corrosion Fatigue Crack Growth of Zr-based Bulk Metallic Glass

Y. Nakai, and Y. Yoshioka
Kobe University, Kobe, JAPAN

1. Introduction

Because amorphous metals have been produced at a cooling rate higher than 10^5 K/s, very thin ribbons or wires could be obtained. Recently, several families of multicomponent metallic alloy, which shows excellent glass forming ability, have been developed. For the alloys, conventional casting, whose cooling rate is lower than 10 K/s, can be applied to produce amorphous alloys. Using the alloy, bulk structural components can be produced, where the alloy is called bulk metallic glass (BMG). The lack of any long-range order and the subsequent absence of microstructures have led to very high strength and very high corrosion resistance [1]. BMG is in a supercooled liquid state at a temperature between the glass-transition temperature, T_g, and the crystallization temperature, T_x, and machine components can be made by precision casting of BMG because of its low shrinkage from the supercooled liquid state to the solid state. Owing to these excellent properties, BMG has received considerable attention as a structural material, especially for small or micromachine components [2]. To ensure the integrity of structures made of BMG, the mechanisms and mechanics of fatigue fracture should be clarified [3-8].

The authors have studied the fatigue crack growth behavior of BMG in air, and the effects of loading frequency and stress ratio were investigated [3,7,8]. It was found from the study that the fatigue crack propagation rate in air was determined by the stress intensity range, ΔK, but was independent of the loading condition, the stress ratio, and the loading frequency, *i.e.*, the crack propagation under cyclic-loading in air is cycle-dependent. Since BMG has free volume, which is excessive volume relative to some reference state, hydrogen atoms may easily enter the space between atoms, which may lead to environment assisted cracking. Suh and Dauskardt, however, showed retarded fatigue crack growth behavior after hydrogen charging [9], while Schroeder and Ritchie, Kawashima et al. reported that the fatigue crack growth rates were as much as three orders of magnitude higher in aqueous 0.5 M NaCl solution compared with corresponding growth rates in air or deionized water [10-13].

In the present study, the effects of frequency and stress ratio on the crack propagation behavior of BMG in aqueous solutions were examined to clarify whether crack propagation is cycle-dependent or time-dependent, and whether it is determined by maximum stress intensity factor, K_{max} or stress intensity range, ΔK. This information is very important not only for clarifying the mechanisms and mechanics of crack propagation, but also for the design and maintenance of machine components.

2. Experimental Procedures

The material for the present study was bulk metallic glass (BMG), $Zr_{55}Cu_{30}Ni_5Al_{10}$ (at%). The tensile strength of the BMG was 1560 MPa, and Young's modulus was 87 GPa. Samples were initially produced in a plate form by high-pressure casting. The plate dimensions were 20 mm wide, 50 mm long, and 2.0 mm thick, and the surface was polished by grinding. Specimens were wire-electrical-discharge machined from the plates. The geometry and dimensions of the specimen are shown in Fig. 1, and the notch width was 0.30 mm. A fatigue pre-crack of 1.6 mm in length was introduced in air prior for crack propagation tests in aqueous environments.

The crack propagation tests under cyclic-loading were conducted under applied-force-range (ΔP)-controlled, or under stress-intensity-range (ΔK)-controlled conditions using a computer-controlled electrohydraulic testing machine. The ΔK-decreasing tests were conducted in accordance with ASTM standard E647, where the applied force range was automatically reduced by the control computer after every 50 μm crack extension. Sinusoidal loading wave with a stress ratio, R of 0.1 or 0.5 and a frequency, f, of 20 or 1.0Hz was employed for the crack propagation tests. The tests were conducted either in aerated 3.5, 0.05, or 0.01% NaCl solutions, or high-purity deionized water. The sustained-load tests were also conducted using the electrohydraulic testing machine. The crack lengths were continuously monitored using a compliance obtained from a backface strain gage.

3. Experimental Results
3.1 Sustained-load Test

The crack growth rate in 3.5% NaCl solution under a sustained load is shown in Fig. 2 together with the results obtained by Schroeder et al. for a Zr-Ti-Ni-Cu-Be BMG [10]. The crack growth rate obtained in the present experiment was almost identical to that by Schroeder et al., both were almost constant in Region II
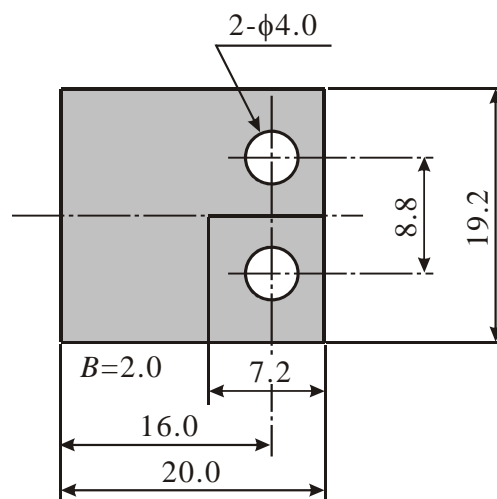
Fig. 1. Shape and dimensions of specimen (in mm).
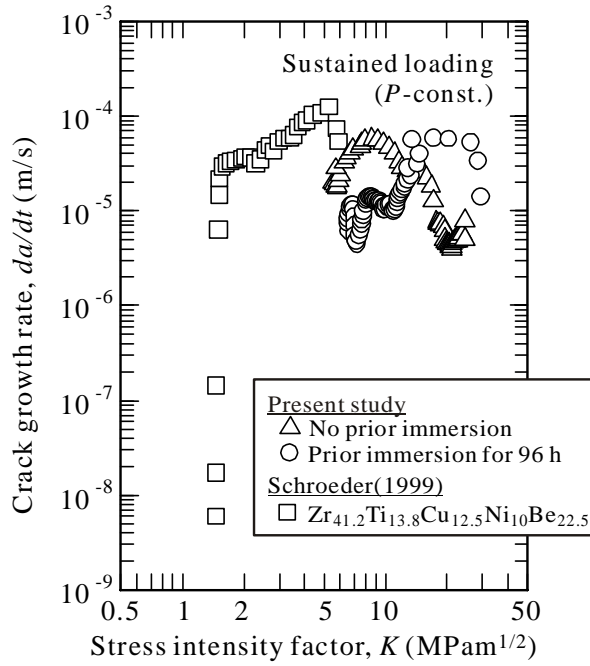
Fig. 2.   Crack growth rate in 3.5 % NaCl solution under sustained-loading.

(a) Cycle-based crack growth rate   (b) Time-based crack growth rate
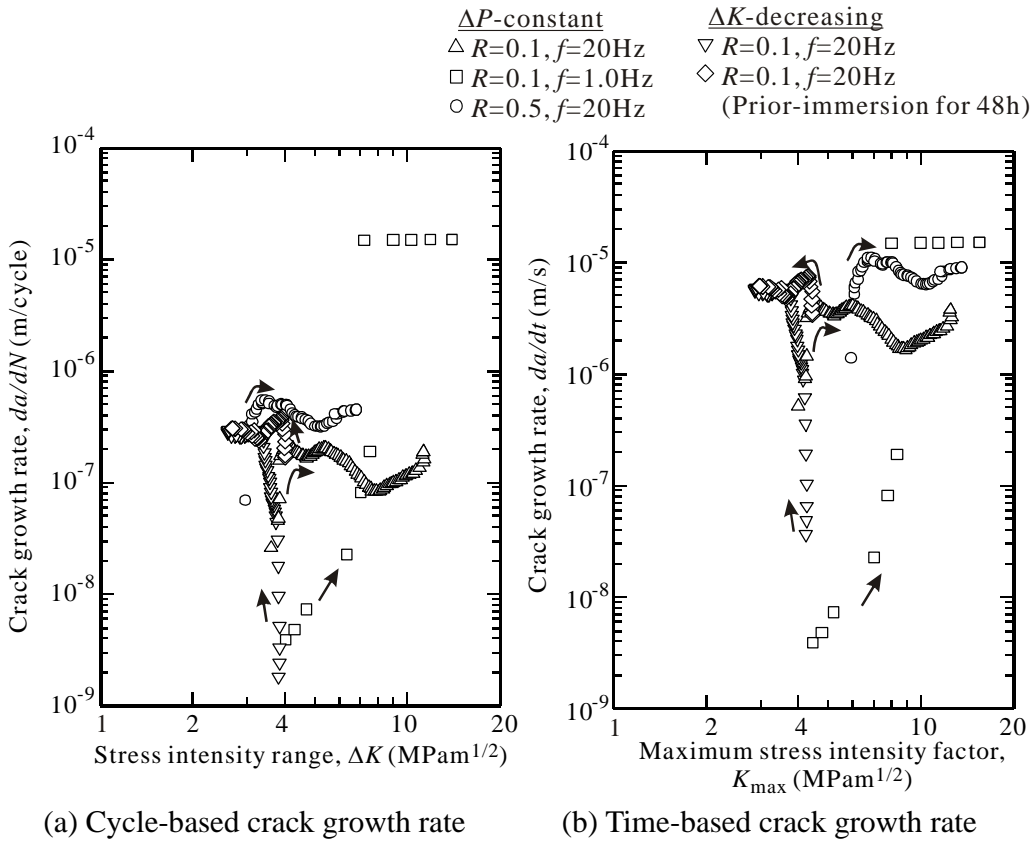
Fig. 3.   Effects of loading frequency and stress ratio on crack growth behavior
in 3.5% NaCl solution under cyclic-loading.

independent of the stress intensity factor K.   The value, $(da/dt)_{II}$ was from 10^{-5} to 10^{-4} m/s.

3.2 Cyclic-loading Test

The effect of loading frequency and the stress ratio on the crack propagation rate in 3.5% NaCl solution is shown in Fig. 3, where (a) and (b) show the da/dN-ΔK and da/dt-K_{max} relationships, respectively.

In case of stress ratio, R=0.1 and loading frequency, f=20Hz, both the constant applied force range (ΔP) tests and ΔK decreasing tests were carried out for specimens without prior-immersion, and only ΔK decreasing tests were conducted for specimens with prior-immersion.   It is clear from these results that the crack propagation behavior just after the start of the tests depended on the loading conditions, and those are determined neither by K_{max} nor ΔK.

As shown by arrows in Fig. 3, the value of ΔK increased with crack growth in the ΔP constant tests, and otherwise, it decreased with crack extension in ΔK decreasing tests.   The crack growth rate just after the start of the tests, however, increased with crack extension in either case without prior-immersion.   After the initial transition, the rate became constant value, which was almost independent of the loading conditions, and regardless to the prior-immersion.   Such transitional behavior was not observed in the result under the static loading tests, where the crack propagation rate seemed to be always constant.

As shown in Fig. 3(a), for the cycle-based crack propagation rate, $(da/dN)_{II}$, at the steady state, there was no difference between the results for f=20Hz obtained by
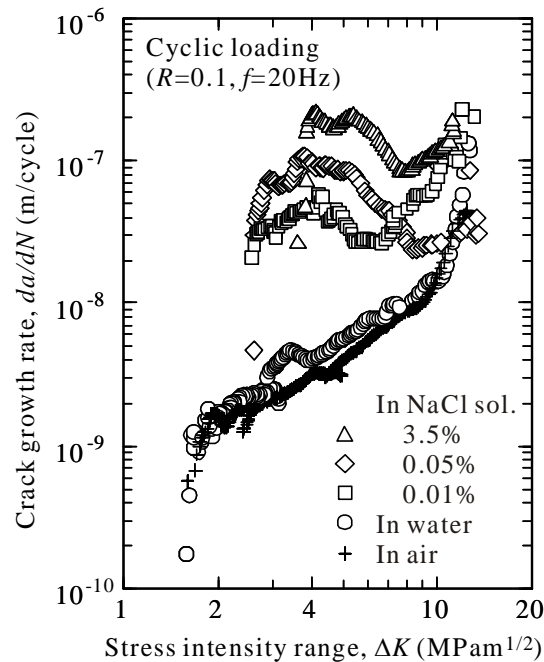
Fig. 4.   Effect of environment on crack growth rate under cyclic-loading.

ΔK decreasing tests and ΔP constant tests. The crack propagation rate was slightly higher for higher stress ratio, while the growth rate for f=1.0Hz was much higher than those for f=20Hz. As shown in Fig. 3 (b), however, the time-based crack growth rate, $(da/dt)_{II}$, for f=1.0Hz was close to that for f=20Hz, and the effect of loading frequency on the time-based crack growth rate $(da/dt)_{II}$ in the steady state region was much smaller than that for the cycles based crack growth rate. The value of $(da/dt)_{II}$ for f=1.0Hz was almost equal to the crack growth rate $(da/dt)_{SCCII}$ in Region II under the sustained-loading tests, which is shown in Fig. 2. The rates for f=20Hz, however, were scarcely lower than those for f=1.0Hz.

Therefore, cracks must grow in 3.5%NaCl aqueous solution by an environment-assisted cracking mechanism. For further detail analysis, studies to clarify whether the crack propagation is determined by the surface chemical reaction rate or the mass transport of bulk environment to the crack tip should be conducted [12,14].

The effect of the environment on the crack propagation for a loading frequency of 20 Hz and a stress ratio of 0.1 is shown in Fig. 4. The da/dN-ΔK relationship for deionized water was almost identical to that in air. In NaCl solution, however, the crack growth rate was higher than that in air even in aqueous solution whose NaCl concentration was very low, *e.g.*, 0.01%, and it was essentially independent of the ΔK level, while it was higher for high concentrations of NaCl.

3.3 Fractography

(a) In air, cyclic-loading
(R=0.1, f=20 Hz)

(b) In high purity water, cyclic-loading
(R=0.1, f=20 Hz)

(c) In 3.5%NaCl sol., sustained-loading

(d) In 0.01%NaCl sol., cyclic-loading
(R=0.1, f=20 Hz)

(e) In 0.05%NaCl sol., cyclic-loading
(R=0.1, f=20 Hz)

(f) In 3.5%NaCl sol., cyclic-loading
(R=0.1, f=20 Hz)
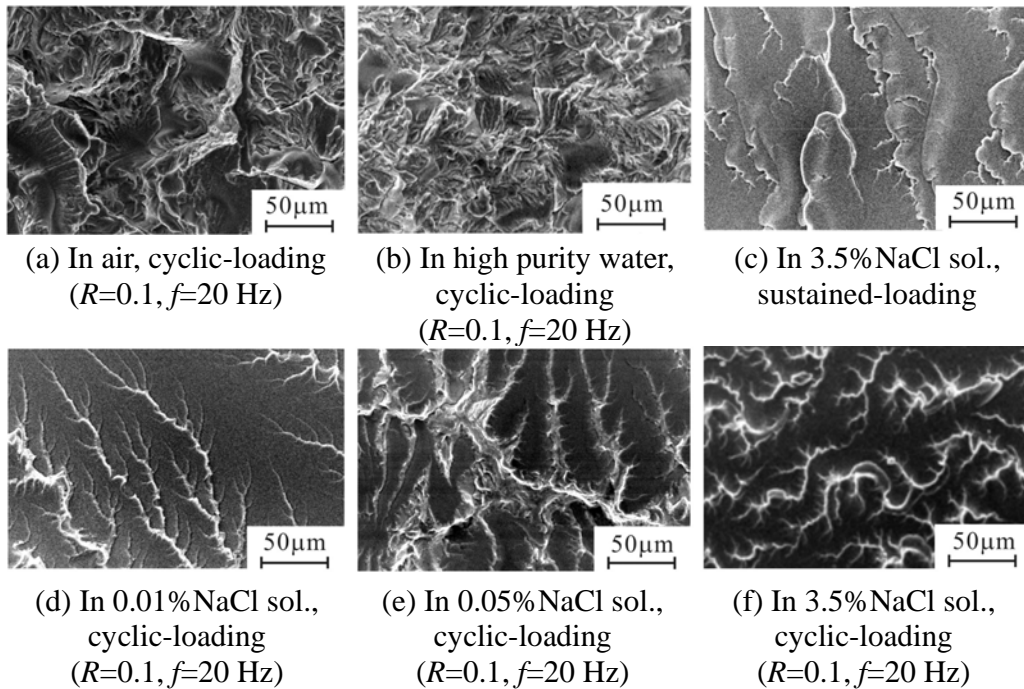
Fig. 5.   Fracture surfaces (Crack propagation direction: Left to right).

Typical morphologies of the fracture surface in each environment are shown in Fig. 5, where the crack propagated from left to right in these figures. The fracture surface generated in deionized water was similar to that generated in air, and those in NaCl solutions were similar to those under a sustained load in the same environment. These observations are consistent with the crack growth behavior, *i.e.*, the crack growth mechanism under cyclic-loading in deionized water was the same as that in air, and the mechanism in the NaCl solutions was similar to that under a sustained load.

The morphologies of the fracture surface in the NaCl solutions were different from that in air, and they were microscopically smooth in the former [12]. These smooth areas were separated by river-pattern-like morphologies. The spacing of the river marks increased with the concentration of NaCl, and it was lower for a sustained load (SCC) than that for a cyclic load (fatigue). Although the smooth areas are cleavage planes for crystalline materials, those in BMG have not been identified.

By using image reconstruction software, Alicona MeX, the three-dimensional shape of the fracture surface was constructed from two SEM images, those were obtained by tilting ±3° from the top. The results of the fracture surface indicated in Fig. 5(e) is displayed in Fig. 6, where the shape and wire frame rendering of the axonometric view is shown in (a), and the shapes of the side views of the fracture surface are demonstrated in (b), (c), and (d). By comparing the SEM graph and three-dimensional reconstruction images, river marks observed in the SEM graph shows steep slopes, and the fracture surfaces in both sides of the patterns are planes with small roughness. As well as in crystalline metals, such river-pattern-like morphology must be formed by the coalescence of cracks those were formed in the different sites.

(a) Axonometric view   (b) Side view from B

(c) Side view from A   (d) Side view from C
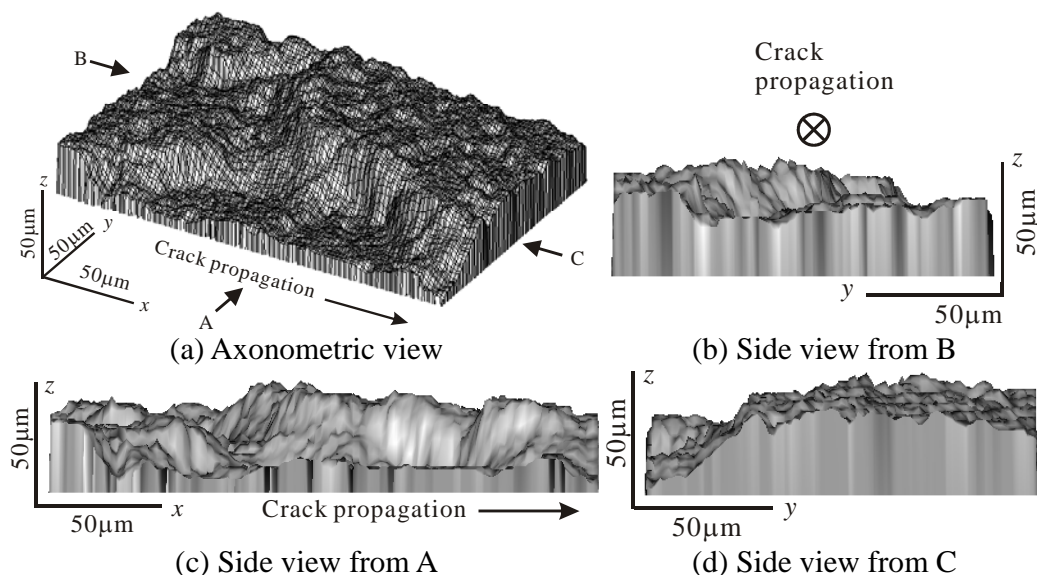
Fig. 6. Three dimensional analysis of fracture surface shown in Fig. 6 (e) (In 0.05% NaCl solution, cyclic-loading, R=0.1, f=20 Hz).

Although the river patterns in crystalline metals are formed by the coalescence of cracks formed along different crystallographic planes (cleavage planes), BMG does not have crystalline structure.   Then in BMG, the orientation of the plane may be determined by the mechanical condition.   Micro-cracks, those were formed along the macroscopic maximum principal stress planes, may have coalesced each other to form the river marks.   The river mark surface seems to be close to the macroscopic maximum shear stress plane because it locates almost 45° from the smooth plane.

4.   Discussion
4.1 Effect of Loading Frequency and Stress Ratio
The crack growth rate in an aggressive environment under cyclic-loading, $(da/dN)_e$, is discussed by Wei [15], and he suggested that it is the sum of three components, one for "pure" fatigue, $(da/dN)_r$, one for the environmental contribution, $(da/dN)_{cf}$, and one is for the sustained-load crack growth, $(da/dN)_{SCC}$, as

$$\left(\frac{da}{dN}\right)_e = \left(\frac{da}{dN}\right)_r + \left(\frac{da}{dN}\right)_{cf} + \left(\frac{da}{dN}\right)_{SCC} \tag{1}$$

The sustained-load contribution appears only in the region where $K_{max} > K_{ISCC}$. Schroeder et al [12]. reported for BMG under cyclic-loading that the sustained-load contribution was dominant, and derived the following equation

$$\left(\frac{da}{dN}\right)_e = \int_0^{1/f} \left(\frac{da}{dt}\right)_{SCC} dt \tag{2}$$

where $(da/dt)_{SCC}$ is a function of the stress intensity factor K, and thus, it is a function of time, t, for a given loading wave.

For $K > K_{ISCC}$, the value of da/dt was almost constant, here, which is expressed as $(da/dt)_{SCCII}$.   Then, Eq. (2) can be rewritten as

$$\left(\frac{da}{dN}\right)_e = \int_0^{t_1} \left(\frac{da}{dt}\right)_{SCC} dt + (t_2 - t_1)\left(\frac{da}{dt}\right)_{SCCII} + \int_{t_2}^{1/f} \left(\frac{da}{dt}\right)_{SCC} dt \tag{3}$$

where t_1 and t_2 are moments at $K = K_{ISCC}$ in the loading and unloading process, respectively.   For $K_{max} \gg K_{ISCC}$, the values of t_1 and $1/f$-t_2 are much smaller than the period of the loading cycle, $1/f$, then, Eq. (3) can be expressed as

$$\left(\frac{da}{dN}\right)_e = (1/f)\left(\frac{da}{dt}\right)_{SCCII} \tag{4}$$

or

$$\left(\frac{da}{dt}\right)_e = \left(\frac{da}{dt}\right)_{SCCII} \tag{5}$$

It means that the time-based crack growth rate under cyclic-loading is given as the rate under sustained-loading when the maximum value of the stress intensity factor at each loading cycle, K_{max}, is much larger than K_{ISCC}.   In addition, Eq. (5) is always valid for high load ratio where $K_{min} > K_{ISCC}$.

These considerations are consistent with the experimental results for R=0.1 and

f=1.0Hz, and R=0.5 and f=20Hz. On the other hand, (da/dt)$_\text{II}$ was slightly lower than (da/dt)$_\text{SCCII}$ for R=0.1 and f=20Hz. Since the fraction of time in one loading period, where the value of K exceeds K_ISCC, is independent of the loading frequency for the similar loading waves such as sinusoidal wave, the difference in the growth rate for 20Hz and 1.0Hz cannot be explained by the above-mentioned mechanism, and other factor(s), such as the effect of the loading frequency on the transport process of solution within cracks, should be considered [15].

4.2 Effect of Prior-immersion

As described in previously, the transitional crack growth behavior was observed just after the start of the test under cyclic-loading of a specimen without prior-immersion, although such transitional behavior did not appeared for a specimen with prior-immersion under cyclic-loading and under sustained-loading regardless to the prior-immersion.

The crack growth behaviors of specimens with and without prior-immersion are
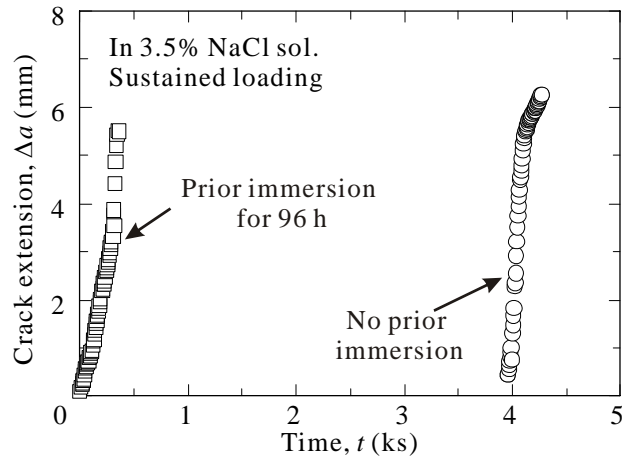
(a) Sustained-loading test
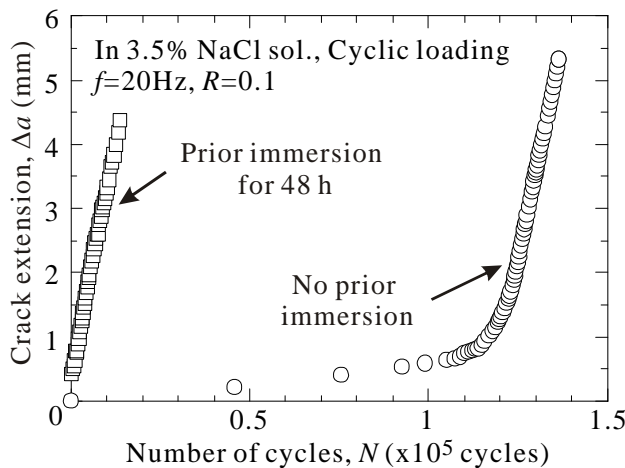
(b) Cyclic-loading test (ΔK decreasing)

Fig. 7. Effect of prior immersion on environment assisted crack growth.

shown in Fig. 7, where (a) is under sustained-loading, and (b) is under cyclic-loading. As shown in Fig. 7 (a), no transitional behavior was observed regardless to the prior-immersion, while the effect of the prior-immersion brought the difference in incubation period, *i.e.*, it was 4ks for a specimen without prior-immersion, and no incubation period for the start of the crack propagation was observed in a specimen with prior-immersion for 96h. It suggests that a crack do not propagate by the SCC mechanism until the concentration of hydrogen atoms at the crack tip reaches a critical value. After start of crack propagation, the steady state behavior was observed.

As shown in Fig. 7(b) for cyclic-loading, no initial transitional crack growth behavior was appeared for a specimen with prior-immersion, contrary to the results for a specimen without prior-immersion. A crack can propagate either by the fatigue or the corrosion fatigue mechanism under cyclic-loading without delay from the start of the loading, *i.e.*, the crack growth by these mechanisms require no incubation period, but the rate are much lower than that by the SCC mechanism. The crack growth during the incubation period of the SCC crack growth must occur by the fatigue mechanism. About 1.2×10^5 cycles (6ks) was required until the start of the steady crack propagation under the cyclic-loading, which was longer than the incubation period under the sustained-loading test. It suggests that the concentration of hydrogen atoms was lower for the former case because the crack tip moved by fatigue mechanisms.

4. Conclusions

In this study, crack propagation tests of a bulk metallic glass, $Zr_{55}Cu_{30}Ni_5Al_{10}$, were conducted either in NaCl solutions or in deionized water, and the following results were obtained.

(1) The crack growth rate in deionized water was almost identical to that in air. The rates in 0.01, 0.05 and 3.5% NaCl solutions, however, were much higher than that in air.

(2) In 3.5% NaCl solution, the time-based crack propagation rate during cyclic-loading, da/dt, was determined by the maximum stress intensity factor, K_{max}, but was almost independent of the loading frequency and the stress ratio, and the growth rate was almost identical to that of environment-assisted cracking under a sustained load.

(3) Initial transitional crack propagation behavior appeared under cyclic-loading, when the loading started just after the immersion of a specimen in the solution, while it was not observed when sufficient prior-immersion was conducted before the loading. The transitional crack propagation behavior, however, did not appear regardless of the prior-immersion under the sustained-loading, while incubation period for crack growth was observed in a specimen without prior-immersion.

Acknowledgments

5. References

[1] C.J. Gilbert, J.M. Lippmann and R.O. Ritchie, Fatigue of Zr-Ti-Cu-Ni-Be bulk amorphous metal: Stress/life and crack-growth behavior, Scripta Materialia, 38 (4) (1998) 537-542

[2] M. Ishida, H. Takeda, N. Nishiyama, K. Amiya, K. Kita, Y. Shimizu, D. Watanabe, E. Fukushima, Y. Saotome, and A. Inoue, World's smallest gear–motor using micro gears made of the bulk metallic glass, Materia Japan, 44 (5) (2005) 431-433

[3] Y. Nakai, S. Hosomi, and M. Seki, Fatigue crack initiation and propagation in Zr-based bulk metallic glass, Proceedings of Fatigue 2006, CD-ROM (2006).

[4] Y. Nakai and S. Hosomi, Fatigue crack initiation and small-crack propagation in Zr-based bulk metallic glass, Materials Transactions, 48 (2007) 1770-1773

[5] Y. Nakai, N. Sei and B.K. Kim, Notched fatigue of Zr-based bulk metallic glass, Key Engineering Materials, 345-346 (2007) 259-262

[6] Y. Nakai, K. Sakai, and K. Nakagawa, Fatigue of Zr-based bulk metallic glass under compression-compression stress, To be published in Advanced Engineering Materials (2008).

[7] Y. Nakai and M. Seki, Effects of stress ratio and frequency on fatigue crack growth behavior of Zr-based bulk metallic glass, Journal of the Society of Materials Science, Japan, 56 (3) (2007) 229-235

[8] Y. Nakai and M. Seki, Mechanisms and mechanics of fatigue crack propagation in Zr-based bulk metallic glass, Key Engineering Materials, 378-379 (2008) 317-328

[9] D. Suh and R.H. Dauskardt, Hydrogen effects on the mechanical and fracture behavior of Zr-Ti-Ni-Cu-Be bulk metallic glass, Scripta Materialia, 42 (3) (2000) 233-240

[10] V. Schroeder, C.J. Gilbert, and R.O. Ritchie, Effect of aqueous environment on fatigue crack propagation behavior in a Zr-based bulk amorphous metal, Scripta Materialia, 40 (9) (1999) 1057-1061

[11] R.O. Ritchie, V. Schroeder and C.J. Gilbert, Fracture, fatigue and environmentally-assisted failure of a Zr-based bulk amorphous metal, Intermetallics, 8 (2000) 469-475

[12] V. Schroeder and R.O. Ritchie, Stress-corrosion fatigue–crack growth in a Zr-based bulk amorphous metal, Acta Materialia, 54 (2006) 1785-1794

[13] A. Kawashima, H. Kurishita, H. Kimura, and A. Inoue, Effect of chloride ion concentration on the fatigue crack growth rate of a $Zr_{55}Al_{10}Ni_5Cu_{30}$ bulk metallic glass, Materials Transactions, 48 (2007) 1969-1972

[14] Y. Nakai, A. Alavi, and R.P. Wei, Effects of frequency and temperature on short fatigue crack growth in aqueous environments, Metallurgical Transactions A, 19 (1988) 543-548

[15] R.P. Wei, On understanding environment-enhanced fatigue crack growth – A fundamental approach, ASTM STP 675 (1979) 816-840